Doping-Induced Ferromagnetism and Possible Triplet Pairing in d^4 Mott Insulators

Jiří Chaloupka[1] and Giniyat Khaliullin[2]
[1]Central European Institute of Technology, Masaryk University, Kotlářská 2, 61137 Brno, Czech Republic
[2]Max Planck Institute for Solid State Research, Heisenbergstrasse 1, D-70569 Stuttgart, Germany
(Received 26 October 2015; published 8 January 2016)

We study the effects of electron doping in Mott insulators containing d^4 ions such as Ru^{4+}, Os^{4+}, Rh^{5+}, and Ir^{5+} with $J = 0$ singlet ground state. Depending on the strength of the spin-orbit coupling, the undoped systems are either nonmagnetic or host an unusual, excitonic magnetism arising from a condensation of the excited $J = 1$ triplet states of t_{2g}^4. We find that the interaction between J excitons and doped carriers strongly supports ferromagnetism, converting both the nonmagnetic and antiferromagnetic phases of the parent insulator into a ferromagnetic metal, and further to a nonmagnetic metal. Close to the ferromagnetic phase, the low-energy spin response is dominated by intense paramagnon excitations that may act as mediators of a triplet pairing.

DOI: 10.1103/PhysRevLett.116.017203

A distinct feature of Mott insulators is the presence of low-energy magnetic degrees of freedom, and their coupling to doped charge carriers plays the central role in transition metal compounds [1]. In large spin systems like manganites, this coupling converts parent antiferromagnet (AF) into a ferromagnetic (FM) metal and gives rise to large magnetoresistivity effects. The doping of spin one-half compounds like cuprates and titanites, on the other hand, suppresses magnetic order and a paramagnetic (PM) metal emerges. In general, the fate of magnetism upon charge doping is dictated by the spin-orbital structure of parent insulators.

In compounds with an even number of electrons on the d shell, one may encounter a curious situation when the ionic ground state has no magnetic moment at all, yet they may order magnetically by virtue of low-lying magnetic levels with finite spin, if the exchange interactions are strong enough to overcome the single-ion magnetic gap. The d^4 ions such as Ru^{4+}, Os^{4+}, Rh^{5+}, Ir^{5+} possess exactly this type of level structure [2] due to spin-orbit coupling $\lambda(\boldsymbol{S}\cdot\boldsymbol{L})$: the spin $S = 1$ and orbital $L = 1$ moments form a nonmagnetic ground state with total $J = 0$ moment, separated from the excited level $J = 1$ by λ. A competition of the exchange and spin-orbit couplings results then in a quantum critical point (QCP) between the nonmagnetic Mott insulator and the magnetic order [3,4]. Since the magnetic order is due to the condensation of the virtual $J = 1$ levels and hence "soft," the amplitude (Higgs) mode is expected. The corollary of the "d^4 excitonic magnetism" [3] is the presence of the magnetic QCP that does not require any special lattice geometry, and the energy scales involved are large. The recent neutron scattering data [5] in d^4 Ca_2RuO_4 seem to support the theoretical expectations.

As we show in this Letter, the unusual magnetism of d^4 insulators, where the soft J spins fluctuate between 0 and 1, results also in anomalous doping effects that differ drastically from conventional cases as manganites and cuprates. Indeed, while common wisdom suggests that the PM phase with yet uncondensed J moments near QCP would get even "more PM" upon doping, we find that mobile carriers induce long-range order instead. The order is of the FM type and is promoted by the carrier-driven condensation of J moments. By the same mechanism, the exchange dominated AF phase also readily switches to the FM metal, as observed in La-doped Ca_2RuO_4 [6,7]. The theory might be relevant also to the electric-field-induced FM of Ca_2RuO_4 [8] and the FM state of the RuO_2 planes in oxide superlattices [9]. Further doping suppresses any magnetic order, and we suggest that residual FM correlations may lead to a triplet superconductivity (SC).

Model.—There are a number of d^4 compounds, magnetic as well nonmagnetic, with various lattice structures [10–17]. To be specific, we consider a square lattice d^4 insulator lightly doped by electrons. Assuming relatively large spin-orbit coupling (SOC), the relevant states are pseudospin $J = 0, 1$ states of t_{2g}^4 and $J = 1/2$ states of t_{2g}^5 [see Fig. 1(a)]. The d^4 singlet s ($J = 0$) and triplon $T_{0,\pm1}$ ($J = 1$) states obey the Hamiltonian derived in Ref. [3]. Adopting the Cartesian basis $T_x = (T_1 - T_{-1})/\sqrt{2}i$, $T_y = (T_1 + T_{-1})/\sqrt{2}$, and $T_z = iT_0$, it can be written as

$$\mathcal{H}_{d^4} = \lambda\sum_i \boldsymbol{T}_i^\dagger\cdot\boldsymbol{T}_i + \frac{1}{4}K\sum_{\langle ij\rangle}\Big[s_i s_j^\dagger\Big(\boldsymbol{T}_i^\dagger\cdot\boldsymbol{T}_j - \frac{1}{3}T_{i\gamma}^\dagger T_{j\gamma}\Big) - s_i^\dagger s_j^\dagger\Big(\frac{5}{6}\boldsymbol{T}_i\cdot\boldsymbol{T}_j - \frac{1}{6}T_{i\gamma}T_{j\gamma}\Big) + \text{H.c.}\Big], \quad (1)$$

where γ is determined by the bond direction. The model shows the AF transition due to a condensation of $\boldsymbol{T}$ at a critical value $K_c = \frac{6}{11}\lambda$ of the interaction parameter $K = 4t_0^2/U$. The degenerate $T_{x,y,z}$ levels split upon material-dependent lattice distortion, affecting the details of the model behavior [18]. We will consider the cubic

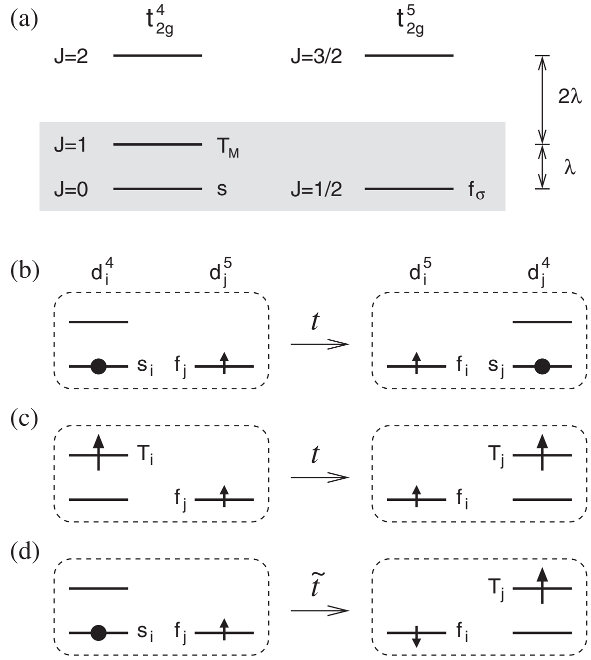

FIG. 1. (a) Spin-orbital level structure of t_{2g}^4 and t_{2g}^5 configurations. The lowest states including singlet s and triplet T_M states of d^4, and pseudospin 1/2 f_σ states of d^5 configurations form a basis for the effective low-energy Hamiltonian. (b)–(d) Schematics of electron hoppings that lead to Eqs. (2) and (3): (b) Free motion of a doped fermion f_σ in a singlet background. (c) The fermion hopping is accompanied by a triplon backflow supporting the double-exchange type ferromagnetism. (d) Fermionic hopping generates a singlet-triplet excitation. This process leads to a coupling between the Stoner continuum and T moments promoting magnetic condensation.

symmetry case and make a few comments on the possible effects of the tetragonal splitting.

The d^4 system is doped by introducing a small number of d^5 objects—fermions f_σ carrying the pseudospin $J = 1/2$ of t_{2g}^5. The on-site constraint $n_s + n_T + n_f = 1$ is implied. The Hamiltonian describing the correlated motion of f is derived by calculating matrix elements of the nearest-neighbor hopping $\hat{T}_{ij} = -t_0(a_{i\sigma}^\dagger a_{j\sigma} + b_{i\sigma}^\dagger b_{j\sigma})$ between multielectron configurations $\langle d_i^5 d_j^4 | \hat{T}_{ij} | d_i^4 d_j^5 \rangle$. Here, a and b are the t_{2g} orbitals active on a given bond, e.g., xy and zx for x bonds. The resulting hopping Hamiltonian comprises three contributions, $\mathcal{H}_{d^4-d^5} = \sum_{ij}(h_1 + h_2 + h_3)_{ij}^{(\gamma)}$. The first one, depicted schematically in Figs. 1(b) and 1(c), is a spin-independent motion of f, accompanied by a backflow of s and $\boldsymbol{T}$:

$$h_1^{(\gamma)} = -t f_{i\sigma}^\dagger f_{j\sigma}\left[s_j^\dagger s_i + \frac{15}{16}\left(\boldsymbol{T}_j^\dagger \cdot \boldsymbol{T}_i - \frac{3}{5} T_{j\gamma}^\dagger T_{i\gamma}\right)\right]. \quad (2)$$

The second contribution is a spin-dependent motion of f generating $J = 0 \leftrightarrow J = 1$ magnetic excitation in the d^4 background [see Fig. 1(d)]:

$$h_2^{(\gamma)} = i\tilde{t}\left[\sigma_{ij}^\gamma (s_j^\dagger T_{i\gamma} - T_{j\gamma}^\dagger s_i) - \frac{1}{3}\boldsymbol{\sigma}_{ij} \cdot (s_j^\dagger \boldsymbol{T}_i - \boldsymbol{T}_j^\dagger s_i)\right]. \quad (3)$$

Here, $\boldsymbol{\sigma}_{ij} = f_{i\alpha}^\dagger \boldsymbol{\tau}_{\alpha\beta} f_{j\beta}$ with Pauli matrices τ denotes the bond-spin operator. The derivation for the cubic symmetry gives $t = \frac{4}{9} t_0$ and $\tilde{t} = (1/\sqrt{6}) t_0$ with the ratio $\tilde{t}/t \approx 1$. However, these values are affected by the lattice distortions (via the pseudospin wave functions) and f-band renormalization reducing the effective t. We thus consider $\tilde{t}/t$ as a free parameter and set $\tilde{t} = 1.5t$ below. The last contribution to $\mathcal{H}_{d^4-d^5}$ reads as coupling between the bond spins residing in f and T sectors: $h_3^{(\gamma)} = \frac{9}{16} t(\sigma_{ij}^\gamma J_{ji}^\gamma + \frac{1}{3}\boldsymbol{\sigma}_{ij} \cdot \boldsymbol{J}_{ji})$, where $\boldsymbol{J}_{ji} = -i(\boldsymbol{T}_j^\dagger \times \boldsymbol{T}_i)$. At small doping and near QCP where the density of $\boldsymbol{T}$ excitons is small, the scattering term h_3 can be neglected.

Phase diagram.—We first inspect the phase behavior of the model as a function of doping x and interaction parameters K and $\tilde{t}$. The magnetic order is linked to the condensation of triplons induced by their mutual interactions and the interaction with the doped fermions f. In contrast to the cubic lattice where all the $\boldsymbol{T}$ flavors are equivalent, on the two-dimensional square lattice the T_z flavor experiences the strongest interactions and is selected to condense, provided that it is not suppressed by a large tetragonal distortion. We thus focus on T_z and omit the index z.

Following the standard notation for spin-1 condensates, we express complex $\boldsymbol{T} = \boldsymbol{u} + i\boldsymbol{v}$ using two real fields $\boldsymbol{u}$, $\boldsymbol{v}$. The ordered dipolar moment residing on Van Vleck transition $s \leftrightarrow \boldsymbol{T}$ is then $\boldsymbol{m} = 2\sqrt{6}\boldsymbol{v}$ [3]. Assuming either FM order (condensation prescribed by $T \to iv$) or AF order ($T \to \pm iv$ in a Néel pattern), we evaluate the classical energy of the T condensate and add the energy of the f bands polarized due to the condensed T. Doing so, we replace s_i by $\sqrt{1 - x - v^2}$ to incorporate the constraint, on average. The resulting total energy $E(v) = E_T + E_{\text{band}}$ is minimized with respect to the condensate strength v and compared for the individual phases: FM, AF, and PM ($v = 0$). The condensate energy amounts to $E_T = [\lambda \pm \frac{11}{6} K(1 - x - v^2)]v^2$, with the + (−) sign for FM (AF) phase, respectively. The band energy $E_{\text{band}} = \sum_{\boldsymbol{k}\sigma} \varepsilon_{\boldsymbol{k}\sigma} n_{\boldsymbol{k}\sigma}$ is calculated for a particular doping level $x = \sum_{\boldsymbol{k}\sigma} n_{\boldsymbol{k}\sigma}$ using the band dispersion $\varepsilon_{\boldsymbol{k}\sigma} = -4(t_1 - \sigma t_2)\gamma_{\boldsymbol{k}}$, where $\gamma_{\boldsymbol{k}} = \frac{1}{2}(\cos k_x + \cos k_y)$. The hopping parameter t_1 stemming from h_1 reads as $t_1 \simeq t(1 - x)$ and $t_1 \simeq t(1 - x - 2v^2)$ for FM and AF, respectively. This captures the double-exchange nature of h_1—only FM-aligned T allow for a free motion of f, while the AF order of T blocks it. The parameter t_2 quantifies the polarization of the bands by virtue of h_2 and is nonzero in the FM case only: $t_2 = \frac{2}{3}\tilde{t} v\sqrt{1 - x - v^2}$.

Shown in Fig. 2 are the resulting phase diagrams along with the total ordered moment $m[\mu_B] = 2\sqrt{6}v + n_\uparrow - n_\downarrow$.

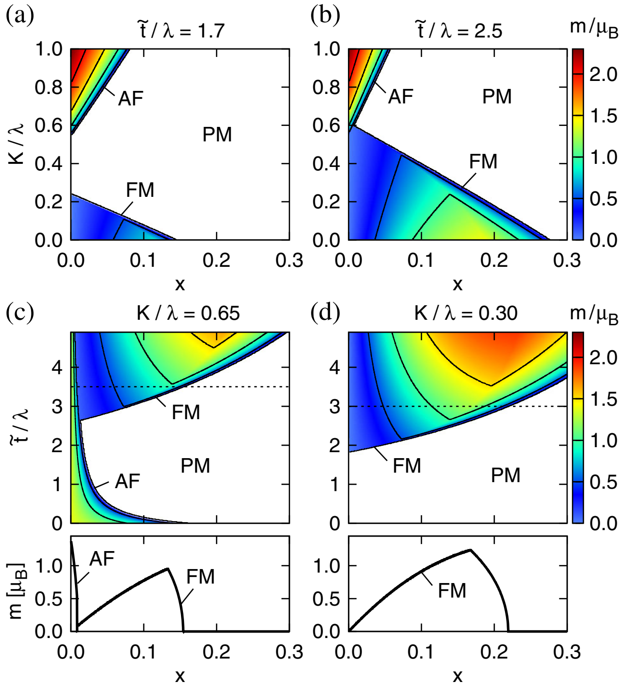

FIG. 2. (a),(b) Phase diagrams and the ordered magnetic moment value for varying doping x and K/λ keeping fixed $\tilde{t}/\lambda$ of 1.7 and 2.5. (c) Phase diagram for varying doping and $\tilde{t}/\lambda$ and fixed $K = 0.65\lambda$ above the critical $K_c = \frac{6}{11}\lambda$ of the d^4 system. The bottom panel shows $m(x)$ along the cut at $\tilde{t}/\lambda = 3.5$. (d) The same for $K = 0.3\lambda$ and the cut at $\tilde{t}/\lambda = 3$.

In both phase diagrams for constant $\tilde{t}/\lambda$ [Figs. 2(a) and 2(b)] at $x = 0$ we recover the QCP of the d^4 model. Nonzero doping causes a suppression of the AF phase via the double-exchange mechanism in h_1, and an appearance of the FM phase strongly supported by h_2 that directly couples the moment $\boldsymbol{m} \sim \boldsymbol{v}$ of $\boldsymbol{T}$ exciton to the fermionic spin $\boldsymbol{\sigma}_{ij}$, promoting magnetic condensation. With an increasing $\tilde{t}$ the FM phase quickly extends as seen also in Figs. 2(c) and 2(d) containing the phase diagrams for constant $K/\lambda = 0.65$ (selected to roughly reproduce the experimental value 1.3 μ_B for Ca_2RuO_4 [19]) and $K/\lambda = 0.30$. The constant $\tilde{t}/\lambda$ cut in Fig. 2(c) is strongly reminiscent of the phase diagram of La-doped Ca_2RuO_4 [6,7,20], where the AF phase is almost immediately replaced by the FM phase present up to a certain doping level. To estimate realistic values of $\tilde{t}/\lambda$, we assume $t_0 \sim 300$ meV. The large SOC in d^4 Ir^{5+} with $\lambda \sim 200$ meV [22–24] leads to $\tilde{t}/\lambda \sim 1$ and places it strictly to the AF/PM (c) or PM/PM (d) regime. In contrast to this, the moderate $\lambda \sim 70$–80 meV in Ru^{4+} [2,25] makes the FM phase easily accessible.

Spin susceptibility, emergence of paramagnons.—The tendency toward FM ordering naturally manifests itself in the dynamic spin response of the coupled $\boldsymbol{T}$ exciton and f-band system. Here we study it in detail for the PM phase, focusing again on T_z being the closest to condense. The magnetic moment $\boldsymbol{m}$ is carried mainly by the dipolar component $\boldsymbol{v} = (\boldsymbol{T} - \boldsymbol{T}^\dagger)/2i$ of triplons so that the dominant contribution to the spin susceptibility is given by the $\boldsymbol{v}$ susceptibility $\chi(\boldsymbol{q}, \omega)$. To evaluate it, we replace $s_i \to \sqrt{1 - x - n_{Ti}}$, and decouple h_1 (3) into f and T parts on a mean-field level. This yields a fermionic Hamiltonian $\mathcal{H}_f = \sum_{\boldsymbol{k}\sigma} \varepsilon_{\boldsymbol{k}} f^\dagger_{\boldsymbol{k}\sigma} f_{\boldsymbol{k}\sigma}$ with $\varepsilon_{\boldsymbol{k}} = -4t(1-x)\gamma_{\boldsymbol{k}}$, and a quadratic form for T_z boson: $\mathcal{H}_T = \sum_{\boldsymbol{q}} [A_{\boldsymbol{q}} T^\dagger_{\boldsymbol{q}} T_{\boldsymbol{q}} - \frac{1}{2} B_{\boldsymbol{q}} (T_{\boldsymbol{q}} T_{-\boldsymbol{q}} + T^\dagger_{\boldsymbol{q}} T^\dagger_{-\boldsymbol{q}})]$. Here, $A_{\boldsymbol{q}} = \lambda + 4t\langle n_{ij}\rangle(1 - \gamma_{\boldsymbol{q}}) + K(1-x)\gamma_{\boldsymbol{q}}$, $B_{\boldsymbol{q}} = \frac{5}{6} K(1-x)\gamma_{\boldsymbol{q}}$, and $\langle n_{ij}\rangle = \sum_{\boldsymbol{k}\sigma} \gamma_{\boldsymbol{k}} n_{\boldsymbol{k}\sigma}$. Bogoliubov diagonalization provides the bare triplon dispersion $\omega_{\boldsymbol{q}} = (A^2_{\boldsymbol{q}} - B^2_{\boldsymbol{q}})^{1/2}$ and the bare v susceptibility $\chi_0(\boldsymbol{q}, \omega) = \frac{1}{2}(A_{\boldsymbol{q}} - B_{\boldsymbol{q}})/[\omega^2_{\boldsymbol{q}} - (\omega + i\delta)^2]$. The susceptibility is further renormalized by the coupling h_2 (3), which can be viewed as an interaction between a dipolar component v of the triplons and the Stoner continuum of f fermions:

$$\mathcal{H}_{\rm int} = g \sum_{\boldsymbol{q}} v_{\boldsymbol{q}} \tilde{\sigma}_{-\boldsymbol{q}}, \qquad \tilde{\sigma}_{-\boldsymbol{q}} = \sum_{\boldsymbol{k}} \Gamma_{\boldsymbol{k}\boldsymbol{q}} f^\dagger_{\boldsymbol{k}+\boldsymbol{q},\alpha} \tau^z_{\alpha\beta} f_{\boldsymbol{k},\beta}. \tag{4}$$

The coupling constant $g = \frac{8}{3}\tilde{t}\sqrt{1-x}$, and the vertex $\Gamma_{\boldsymbol{k}\boldsymbol{q}} = \frac{1}{2}(\gamma_{\boldsymbol{k}} + \gamma_{\boldsymbol{k}+\boldsymbol{q}})$ is close to 1 in the limit of small $\boldsymbol{k}$, $\boldsymbol{q}$. By treating this coupling on a RPA level, we arrive at the full v susceptibility $\chi = \chi_0/(1 - \chi_0\Pi)$ with the v self-energy

$$\Pi(\boldsymbol{q}, \omega) = g^2 \sum_{\boldsymbol{k}\sigma} \Gamma^2_{\boldsymbol{k}\boldsymbol{q}} \frac{n_{\boldsymbol{k}\sigma} - n_{\boldsymbol{k}+\boldsymbol{q}\sigma}}{\varepsilon_{\boldsymbol{k}+\boldsymbol{q}} - \varepsilon_{\boldsymbol{k}} - \omega - i\delta}. \tag{5}$$

The interplay of the coupled excitonic and band spin responses is demonstrated in Fig. 3. The high-energy component of χ linked to χ_0 follows the bare triplon dispersion $\omega_{\boldsymbol{q}}$. In an undoped system, due to the AF K interaction, $\omega_{\boldsymbol{q}}$ has a minimum at $\boldsymbol{q} = (\pi, \pi)$ and χ_0 would be most intense there. By doping, the double exchange mechanism in h_1 disfavoring AF correlations pushes $\omega_{\boldsymbol{q}}$ up near (π, π). Further, due to a dynamical mixing [Eqs. (3) and (4)] of triplons with the fermionic continuum, the low-energy component of χ gains spectral weight as $\tilde{t}/\lambda$ approaches the critical value, and a gradually softening FM paramagnon is formed [see Fig. 3(b)]. The emergence of the paramagnon and the increase of its spectral weight is shown in detail in Fig. 3(e). Finally, once the critical $\tilde{t}/\lambda$ is reached, triplons, whose spectral weight was pulled down by the coupling to the Stoner continuum, condense and the FM order sets in, signaled by the divergence of $\chi(\boldsymbol{q} = 0, \omega = 0)$ [cf. Figs. 3(c) and 3(d)].

Triplet pairing.—Intense paramagnons emerging in the proximity to the FM phase may serve as mediators of a triplet pairing interaction [26]. In the following, we perform semiquantitative estimates for this triplet SC.

While the dominant contribution to the pairing strength is due to the v_z fluctuations, in order to assess the structure of the triplet order parameter, the full coupling $\mathcal{H}_{\rm int} = g\sum_{\boldsymbol{q}} \boldsymbol{v}_{\boldsymbol{q}} \cdot \tilde{\boldsymbol{\sigma}}_{-\boldsymbol{q}}$ leading to the effective interaction $-\frac{1}{2} g^2 \sum_{\boldsymbol{q}\alpha} \chi_\alpha(\boldsymbol{q}, \omega = 0) \tilde{\sigma}^\alpha_{\boldsymbol{q}} \tilde{\sigma}^\alpha_{-\boldsymbol{q}}$ has to be considered. The

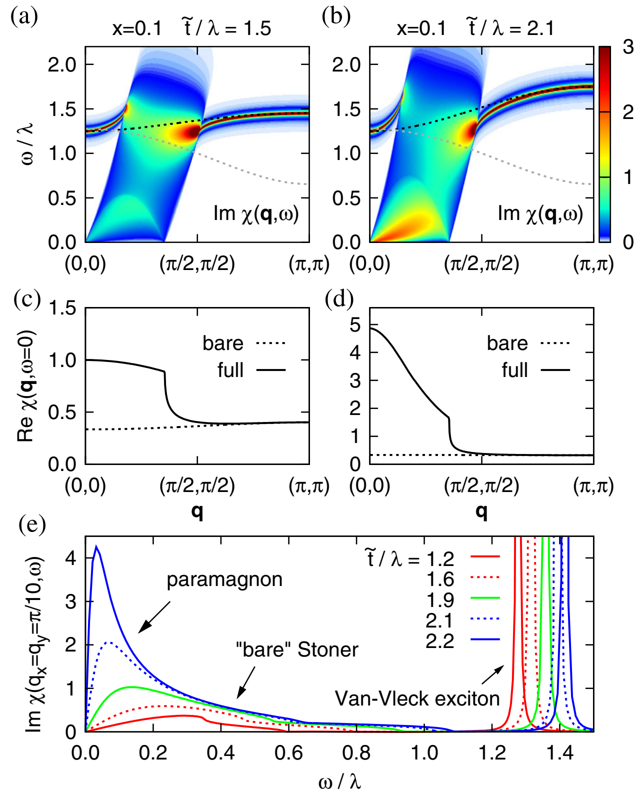

FIG. 3. (a) Imaginary part of the v_z susceptibility $\chi(\boldsymbol{q},\omega)$ in the (π,π) direction calculated for $x=0.1$, $\tilde{t}/\lambda=1.5$, $K/\lambda=0.3$. $\chi(\boldsymbol{q},\omega)$ is shown in units of λ^{-1}. The black (gray) dashed line shows the bare triplon dispersion for $x=0.1$ $(x=0)$. (b) The same for $\tilde{t}/\lambda=2.1$ closer to the FM transition point $\tilde{t}/\lambda\approx 2.25$. (c),(d) The static susceptibility corresponding to panels (a) and (b). (e) Imaginary part of $\chi(\boldsymbol{q},\omega)$ at $\boldsymbol{q}=(\pi/10,\pi/10)$ for several values of $\tilde{t}/\lambda$ gradually approaching the FM transition point.

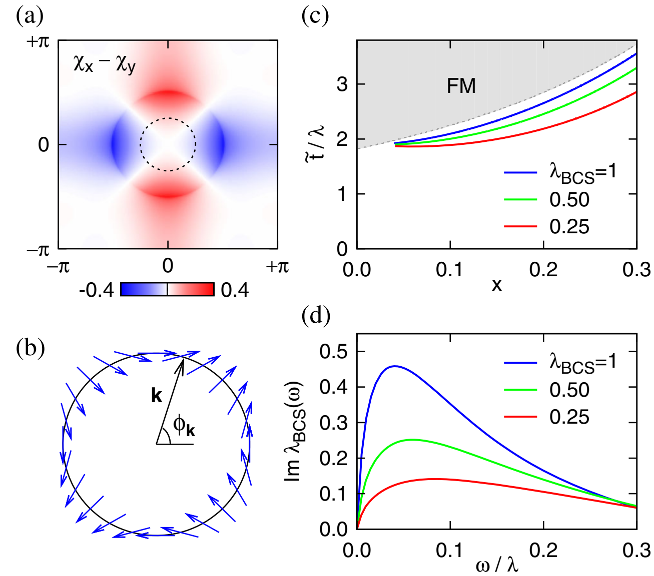

FIG. 4. (a) Combination $(\chi_x-\chi_y)_{\omega=0}$ that determines the symmetry of the pairing potential V_x-V_y. The parameters are the same as in Figs. 3(b) and 3(d). The dashed circle indicates the Fermi surface. (b) Representation of $\Delta_{\pm 1\boldsymbol{k}}=\Delta e^{\pm i\phi_{\boldsymbol{k}}}$ using the $\boldsymbol{d}$ vector along the Fermi surface. (c) Contours of $\lambda_{\mathrm{BCS}}=V_0N$ in the phase diagram of Fig. 2(d). (d) Imaginary part of ω-dependent $\lambda_{\mathrm{BCS}}(\omega)$ for $x=0.1$ and the values of $\tilde{t}/\lambda$ corresponding to $\lambda_{\mathrm{BCS}}=1$, 0.5, and 0.25.

v_α susceptibility χ_α for $\alpha=x,y$ may be calculated the same way as χ_z above, using now $A^\alpha_{\boldsymbol{q}}=A^z_{\boldsymbol{q}}+[\frac{6}{5}t\langle n_{ij}\rangle-\frac{1}{6}K(1-x)]\cos q_\alpha$ and $B^\alpha_{\boldsymbol{q}}=B^z_{\boldsymbol{q}}-\frac{1}{12}K(1-x)\cos q_\alpha$. The coupling vertex for v_x and v_y obtains an additional contribution, $\Gamma^\alpha_{\boldsymbol{kq}}=\Gamma^z_{\boldsymbol{kq}}-\frac{3}{4}[\cos k_\alpha+\cos(k_\alpha+q_\alpha)]$. The resulting BCS interaction in terms of $t_{+1\boldsymbol{k}}=f_{\boldsymbol{k}\uparrow}f_{-\boldsymbol{k}\uparrow}$, $t_{0\boldsymbol{k}}=\frac{1}{\sqrt{2}}(f_{\boldsymbol{k}\downarrow}f_{-\boldsymbol{k}\uparrow}+f_{\boldsymbol{k}\uparrow}f_{-\boldsymbol{k}\downarrow})$, and $t_{-1\boldsymbol{k}}=f_{\boldsymbol{k}\downarrow}f_{-\boldsymbol{k}\downarrow}$ takes the form

$$\begin{aligned}\mathcal{H}_{\mathrm{BCS}}=-\frac{1}{2}\sum_{\boldsymbol{kk}'}[&V_z(t_1^\dagger t_1+t_{-1}^\dagger t_{-1})_{\boldsymbol{kk}'}\\&+(V_x-V_y)(t_1^\dagger t_{-1}+t_{-1}^\dagger t_1)_{\boldsymbol{kk}'}\\&+(V_x+V_y-V_z)t_{0\boldsymbol{k}}^\dagger t_{0\boldsymbol{k}'}],\end{aligned}\tag{6}$$

where V_α denotes the properly symmetrized $V_{\alpha\boldsymbol{kk}'}=g^2(\Gamma^\alpha_{\boldsymbol{k},\boldsymbol{k}'-\boldsymbol{k}})^2\frac{1}{2}[\chi_\alpha(\boldsymbol{k}-\boldsymbol{k}')-\chi_\alpha(\boldsymbol{k}+\boldsymbol{k}')]$. Decomposed into the Fermi surface harmonics, the BCS interaction is well approximated by $V_{z\boldsymbol{kk}'}\approx 2V_0\cos(\phi_{\boldsymbol{k}}-\phi_{\boldsymbol{k}'})$ and $(V_x-V_y)_{\boldsymbol{kk}'}\approx 2V_1\cos(\phi_{\boldsymbol{k}}+\phi_{\boldsymbol{k}'})$ with $V_{0,1}>0$ [see Figs. 3(d) and 4(a)]. The relatively small $V_1\ll V_0$ fixes the relative phase of the t_{+1} and t_{-1} pairs so that the SC order parameter becomes $\Delta_{\pm 1\boldsymbol{k}}=\Delta e^{\pm i\phi_{\boldsymbol{k}}}$. This ordering type is captured by the $\boldsymbol{d}$ vector $\boldsymbol{d}=-i\Delta(\sin\phi_{\boldsymbol{k}},\cos\phi_{\boldsymbol{k}},0)\sim\hat{x}k_y+\hat{y}k_x$ shown in Fig. 4(b). In the classification of Ref. [28], it forms the Γ_4^- irreducible representation of tetragonal group D_{4h}. However, this result applies to the cubic symmetry case. Lattice distortions that cause splitting among $T_{x,y,z}$ and modify the pseudospin wave functions may in fact offer a possibility to "tune" the symmetry of the order parameter. If distortions favor $T_{x,y}$, the potentials $V_{x,y}$ are expected to dominate in Eq. (6), supporting the chiral t_0 pairing represented by the last term in (6).

Data in Figs. 4(c) and 4(d) serve as a basis for a rough T_c estimate. Figure 4(c) shows the BCS parameter $\lambda_{\mathrm{BCS}}\approx V_0N$ (N is DOS per spin component of the f band) which attains sizable values near the FM phase boundary, where the paramagnons are intense. To avoid complex physics near the very vicinity of the FM QCP [29–31], we take a conservative upper limit $\lambda_{\mathrm{BCS}}\approx 0.5$. Extending V_0 by the ω dependence of the underlying $\chi_z(\boldsymbol{q},\omega)$, we define $\lambda_{\mathrm{BCS}}(\omega)$. Its imaginary part to be understood as the conventional α^2F is plotted in Fig. 4(d) yielding an estimate of the BCS cutoff $\Omega\lesssim 0.1\lambda$. With $\lambda\sim 100$ meV, this gives $T_c\approx\Omega e^{-1/\lambda_{\mathrm{BCS}}}$ of about 10 K.

In conclusion, we have explored the doping effects in spin-orbit d^4 Mott insulators. The results show that the doped electrons moving in the d^4 background firmly favor ferromagnetism, explaining, e.g., the observed behavior of

La-doped Ca_2RuO_4. In the paramagnetic phase near the FM QCP, the incipient FM correlations are manifested by intense paramagnons that may provide a triplet pairing.

We thank G. Jackeli for useful comments. J. C. acknowledges support by the Czech Science Foundation (GA ČR) under Project No. 15-14523Y and ERDF under Project CEITEC (CZ.1.05/1.1.00/02.0068).

[1] M. Imada, A. Fujimori, and Y. Tokura, Rev. Mod. Phys. **70**, 1039 (1998).

[2] A. Abragam and B. Bleaney, *Electron Paramagnetic Resonance of Transition Ions* (Clarendon, Oxford, 1970).

[3] G. Khaliullin, Phys. Rev. Lett. **111**, 197201 (2013).

[4] O. N. Meetei, W. S. Cole, M. Randeria, and N. Trivedi, Phys. Rev. B **91**, 054412 (2015).

[5] A. Jain, M. Krautloher, J. Porras, G. H. Ryu, D. P. Chen, D. L. Abernathy, J. T. Park, A. Ivanov, J. Chaloupka, G. Khaliullin, B. Keimer, and B. J. Kim, arXiv:1510.07011.

[6] G. Cao, S. McCall, V. Dobrosavljevic, C. S. Alexander, J. E. Crow, and R. P. Guertin, Phys. Rev. B **61**, R5053 (2000).

[7] G. Cao, C. S. Alexander, S. McCall, J. E. Crow, and R. P. Guertin, J. Magn. Magn. Mater. **226–230**, 235 (2001).

[8] F. Nakamura, M. Sakaki, Y. Yamanaka, S. Tamaru, T. Suzuki, and Y. Maeno, Sci. Rep. **3**, 2536 (2013).

[9] C. R. Hughes, T. Harada, R. Ashoori, A. V. Boris, H. Hilgenkamp, M. E. Holtz, L. Li, J. Mannhart, D. A. Muller, D. G. Schlom, A. Soukiassian, X. Renshaw Wang, and H. Boschker (unpublished).

[10] S. Nakatsuji, S. Ikeda, and Y. Maeno, J. Phys. Soc. Jpn. **66**, 1868 (1997).

[11] Y. Miura, Y. Yasui, M. Sato, N. Igawa, and K. Kakurai, J. Phys. Soc. Jpn. **76**, 033705 (2007).

[12] M. Bremholm, S. E. Dutton, P. W. Stephens, and R. J. Cava, J. Solid State Chem. **184**, 601 (2011).

[13] G. Cao, T. F. Qi, L. Li, J. Terzic, S. J. Yuan, L. E. DeLong, G. Murthy, and R. K. Kaul, Phys. Rev. Lett. **112**, 056402 (2014).

[14] Y. Shi, Y. Guo, Y. Shirako, W. Yi, X. Wang, A. A. Belik, Y. Matsushita, H. L. Feng, Y. Tsujimoto, M. Arai, N. Wang, M. Akaogi, and K. Yamaura, J. Am. Chem. Soc. **135**, 16507 (2013).

[15] P. Khalifah, R. Osborn, Q. Huang, H. W. Zandbergen, R. Jin, Y. Liu, D. Mandrus, and R. J. Cava, Science **297**, 2237 (2002).

[16] S. Lee, J.-G. Park, D. T. Adroja, D. Khomskii, S. Streltsov, K. A. McEwen, H. Sakai, K. Yoshimura, V. I. Anisimov, D. Mori, R. Kanno, and R. Ibberson, Nat. Mater. **5**, 471 (2006).

[17] Hua Wu, Z. Hu, T. Burnus, J. D. Denlinger, P. G. Khalifah, D. G. Mandrus, L.-Y. Jang, H. H. Hsieh, A. Tanaka, K. S. Liang, J. W. Allen, R. J. Cava, D. I. Khomskii, and L. H. Tjeng, Phys. Rev. Lett. **96**, 256402 (2006).

[18] A. Akbari and G. Khaliullin, Phys. Rev. B **90**, 035137 (2014).

[19] M. Braden, G. André, S. Nakatsuji, and Y. Maeno, Phys. Rev. B **58**, 847 (1998).

[20] For a detailed comparison, one has to keep in mind polaronic and phase coexistence effects [21] generic to weakly doped Mott insulators, and deviations from two dimensionality.

[21] W. Brzezicki, A. M. Oleś, and M. Cuoco, Phys. Rev. X **5**, 011037 (2015).

[22] B. N. Figgis and M. A. Hitchman, *Ligand Field Theory and Its Applications* (Wiley-VCH, New York, 2000).

[23] J. Kim, D. Casa, M. H. Upton, T. Gog, Y.-J. Kim, J. F. Mitchell, M. van Veenendaal, M. Daghofer, J. van den Brink, G. Khaliullin, and B. J. Kim, Phys. Rev. Lett. **108**, 177003 (2012).

[24] Note a relation $\lambda = \xi/2S$ between spin-orbit coupling constant λ for spin $S = 1$ and the single-electron one ξ [2].

[25] T. Mizokawa, L. H. Tjeng, G. A. Sawatzky, G. Ghiringhelli, O. Tjernberg, N. B. Brookes, H. Fukazawa, S. Nakatsuji, and Y. Maeno, Phys. Rev. Lett. **87**, 077202 (2001).

[26] We recall that the pseudospins are spin-orbit entangled objects [27], and hence a pseudospin triplet is in fact a mixture of real-spin singlets and triplets.

[27] G. Khaliullin, Prog. Theor. Phys. Suppl. **160**, 155 (2005).

[28] M. Sigrist and K. Ueda, Rev. Mod. Phys. **63**, 239 (1991).

[29] A. V. Chubukov, A. M. Finkel'stein, R. Haslinger, and D. K. Morr, Phys. Rev. Lett. **90**, 077002 (2003).

[30] A. V. Chubukov, C. Pépin, and J. Rech, Phys. Rev. Lett. **92**, 147003 (2004).

[31] A. V. Chubukov and D. L. Maslov, Phys. Rev. Lett. **103**, 216401 (2009).